Ultrasensitive Detection of Carcinoembryonic Antigen by Chitosan/Polythiophene/CdTe Electrochemical Biosensor

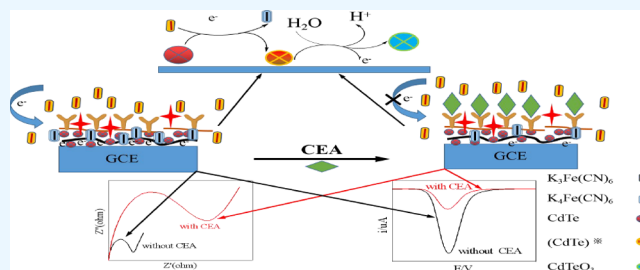Jiajia Wang, Xin Hua, and Baokang Jin*

ACCESS | Metrics & More | Article Recommendations | Supporting Information

ABSTRACT: A facile method for the in situ fabrication of chitosan/polythiophene/CdTe (CS/PTh/CdTe) nanocomposite has been developed. It was then connected with anti-CEA (Ab), which was evoked for the electrochemical detection of carcinoembryonic antigen (CEA, Ag) within $K_4Fe(CN)_6$. The results indicate that CS/PTh/CdTe/GCE has a high selectivity for the detection of CEA with a wide linear range of 0.0001−10000 ng/mL and excellent sensitivity with a low detection limit of 40 fg/mL. Cyclic voltammetry (CV), electrochemical impedance spectroscopy (EIS), X-ray photoelectron spectroscopy (XPS), and in situ FT-IR spectra are evoked to study the mechanism of detection of CEA via CS/PTh/CdTe/GCE. The high sensitivity of the electrochemical sensor is due to the fact that the electrochemical oxidation products of $K_4Fe(CN)_6$ can directly oxidize CdTe from a low energy state to a high energy state $(CdTe)^*$, making CdTe more prone to be oxidized and facilitate electron transfer. The developed electrochemical biosensor can be used for the detection of real samples, providing a precise method for the detection of CEA with potential application in the clinical detection of tumors.

1. INTRODUCTION

Carcinoembryonic antigen (CEA) is a type of highly glycosylated protein that exists in many cancers, including liver cancer, lung cancer, pancreatic carcinoma, colorectal carcinoma, and breast carcinoma. It is recognized as a tumor marker because an obvious increase of CEA is generally presented in malignant tumors.[1−5] Accordingly, CEA detection is extensively utilized in the early clinical diagnosis of cancer, the monitoring of cancer progression, and the therapeutic efficiency evaluation of malignant tumors.[6−10] To date, many techniques for detecting CEA such as electrochemiluminescence, electrophoresis-chemiluminescence, surface-enhanced Raman scattering (SERS), fluorescence, and colorimetric have been well developed.[11−16] For example, Zhu et al. proposed a method for the ultrasensitive detection of CEA by MALDI-TOF mass spectrometry.[17] Su et al. developed a surface plasmon resonance-based methodology for the detection of CEA.[18] Qiu et al. reported a method based on SERS for qualifying a low abundance of CEA.[19] However, these methods are restricted in practical applications due to their high dependence on precise instruments, fussy operation procedures, time-consumption, and limited sensitivity. Therefore, developing a convenient, rapid, and sensitive analytical method for the detection of CEA in serum is of great significance in the early diagnosis and treatment evaluation of cancer.

Electrochemical detection of CEA via biosensors has attracted increasing attention due to its simple equipment, facile operation, high selectivity, economical value, high sensitivity, short diagnostic time, fast response, and ease of miniaturization.[20−22] Enzymes are generally utilized as labels of immunosensor for the detection of CEA, while washing and separation procedures involved during the labeling process unavoidably reduced the stabilities of the enzymes to make labeled immunosensor-based CEA chemical detection a nonrepeatable process.[23,24] Thereby, a label-free biosensor without labeling of enzymes becomes a promising alternative for the electrochemical quantification of CEA.[25,26] However, the nonselective adsorption of antigen and the low sensitivity of the unlabeled biosensor greatly restrict the precise detection of CEA.

Beneficial from the development of nanotechnologies, carbon-based materials such as carbon nanotubes (CNTs),[27] graphene oxide,[28] and metallic nanoparticles including Au nanoparticles[29] and Ag nanoparticles[30] have been extensively utilized as nanocarriers of biosensors for amplifying their sensitivity due to their high specific surface area, excellent electrical conductivity, and remarkable biocompatibility. There are limitations of electron transfers via modification of the biosensor that still exist, reducing the detecting signals of CEA.

As compared to these nanomaterials, quantum dots (QDs) are more attractive semiconductors with an average diameter of 2−20 nm because of their high fluorescence efficiency[31,32] and unique quantum size effect.[33,34] Recently, QDs with a remarkable optoelectronic property, especially II−VI semiconductors containing CdS, CdSe, and CdTe, have been extensively utilized as electrochemiluminescence reagents in bioanalytical applications.[35,36] However, most QDs have poor biocompatibility, hindering their bioanalytical applications.

Organic/inorganic hybridization is a feasible approach for surface modifications of QDs because their carboxyl functional groups on the surface of QDs can form covalent bonds with amino-functionalized molecules. Among them, conductive polymers such as polythiophene (PTh), polypyrrole (PPy), and polyaniline (PANi) are more attractive due to their good optoelectrical effects, remarkable biocompatibility, and easy fabrication properties.[37,38] Meanwhile, chitosan (CS), a positively charged natural polysaccharide with abundant hydroxyl and amino groups, is beneficial for the selective adsorption of antibody and dispersion of PTh/CdTe, as well as for improving the sensitivity of the biosensors for the detection of CEA.[39−41] To the best of our knowledge, there are no published data for the application of CS/PTh/CdTe as the platform and the signal probes in the fabrication of an electrochemical biosensor.

On this basis, a facile in situ ultrasonic copolymerization approach for the fabrication of CS encapsulated PTh/CdTe (CS/PTh/CdTe) electrode has been reported. The CS/PTh/CdTe biosensor has been utilized for the detection of CEA by immobilizing CEA antibody specific recognition. To explore how CS/PTh/CdTe/GCE amplify the electrochemical signal during CEA detection, CV and SWV scanning combined with in situ FT-IR spectroelectrochemistry and XPS are employed. Parameters affecting CEA detection including the concentrations of CS/PTh/CdTe and $K_4Fe(CN)_6$, the reaction temperature, and the reaction time have been optimized to further improve the sensitivity and selectivity of CEA detection.

2. EXPERIMENTAL SECTION

2.1. Materials. TeO_2, KH_2PO_4, NaCl, $CdCl_2 \cdot 2.5H_2O$, bovine serum albumin (BSA), and L-ascorbic acid (AC) were all purchased from Shanghai Aladdin Reagent Co., Ltd. KCl, NaOH, Na_2HPO_4, thiophene (Th), and glutaraldehyde (GA) were obtained from Shanghai Macklin Biochemical Co., Ltd. Interleukin-6 (IL-6) and IL-6 antibody, MUC1, CEA, and CEA antibody were bought from Sangon Biotech (Shanghai) Co., Ltd. L(+)-Cysteine (L-Cys), HNO_3, $K_4Fe(CN)_6$, $K_3Fe-(CN)_6$, acetic acid, and ethanol were bought from Sinopharm Chemical Reagent Co., Ltd. $NaBH_4$ was supplied from Shanghai Energy Chemical Co., Ltd. EIS electrolyte solution consisted of 5.0 mM $[Fe(CN)_6]^{3−/4−}$ containing 0.1 M KCl, and the frequency range was 0.1−100 kHz with a signal amplitude of 5 mV using a Thales electrochemical workstation. All reagents were of analytical grade and used as obtained without further purification. The solutions were all prepared with deionized water (DI water) (18.2 MΩ cm).

2.2. Apparatus. The following were used: vacuum drying oven (Jinghong Laboratory Co. Ltd., Shanghai, China); BGZ series heating and drying oven (Boxun Industry & Commerce Co. Ltd., Shanghai, China); analytical balance (Huazhi Scientific Instrument Co., Ltd., Fujian, China); ultrasonic cleaners (Kunshan Ultrasonic Instrument Co., Ltd., Suzhou,

China); ultra high-resolution scanning electron microscope (Regulus 8230, Hitachi, Japan); supercentrifuge (Xiangyi Centrifuge Instrument Co., Ltd., Hunan, China); rotator (Joanlab, Ningbo, China); electrochemical workstation (CHI 660D, CH Instrument Co., Ltd., Shanghai, China); X-ray diffraction (XRD, Rigaku D/max-rA, 40 kV/100 mA, Japan); scanning electron microscope (SEM) (S-4800, Hitachi, Japan); Thales electrochemical workstation (IM6, Zahner, Germany); Fourier transform infrared spectrometer (FTIR) (Nicolet iS50, Nicolet Instrument Co., Ltd., U.S.); and X-ray photoelectron spectroscopy (XPS, Escalab 250Xi, U.S.).

2.3. Preparation of PTh/CdTe Nanocomposite. Water-soluble PTh/CdTe nanocomposite were prepared following a modified hydrothermal growth method:[33,42,43] First, 0.0319 g (0.2 mmol) of TeO_2 powder was mixed with 10.0 mL of NaOH aqueous solution (0.4 mM) with stirring to form Na_2TeO_3. The Na_2TeO_3 solution as-formed was diluted with 20.0 mL of DI water and 10.0 mL of ethanol. 256 μL of Th solution was then added into a diluted Na_2TeO_3 solution under N_2 atmosphere and kept stirring at 25 °C until it turned transparent. Afterward, 0.2 mM $NaBH_4$ was added into the mixture and continuously stirred for 12 h. 0.6 mM $NaBH_4$ was then added until the mixture changed to pink wool via flocculation.

Second, 2 mM of $CdCl_2 \cdot 2.5H_2O$ and 0.485 g of L-Cys were dissolved into 120 mL of DI water at 25 °C and stirred under N_2 atmosphere for 0.5 h. The pH value of the mixture was adjusted to 11 by the addition of 1.0 M NaOH aqueous solution. The pink PTh/NaHTe flocculation was then reacted with the above mixture in N_2 atmosphere at 25 °C for 0.5 h.

Finally, the mixture was hydrothermally reacted in a polytetrafluoroethylene lined autoclave at 90 °C for 2.5 h. The precipitate obtained was centrifuged, washed, and vacuum-dried at 37 °C to obtain PTh/CdTe nanocomposite. For comparison, pure CdTe and PTh were synthesized as reported.[33,42,44]

2.4. Preparation of CS/PTh/CdTe Nanocomposite. 1.0 mg of CS was dissolved in 1% (v/v) acetic acid aqueous solution to obtain a 1% (m/v) CS solution. Afterward, 1.0 mg of PTh/CdTe particles was ultrasonically dispersed into 5.0 mL of CS solution at 25 °C for 1 h to form a CS/PTh/CdTe hydrogel.[45] The hydrogel was then immersed into 0.5% (m/v) NaOH aqueous solution to remove residual acetic acid and washed with DI water until the pH value turned to 7. The composite materials were finally vacuum-dried at 37 °C to obtain pure CS/PTh/CdTe.

2.5. Fabrication of Electrochemical Immunosensor. First, the glassy carbon electrode (GCE, 3 mm) was polished with 1.0, 0.3, and 0.05 μm α-Al_2O_3 powder sequentially to obtain a mirror-like surface. The polished GCE was then sonicated in DI water, ethanol, and DI water, alternately, and dried in N_2. Afterward, it was modified with 10 μL of CS/PTh/CdTe nanocomposite solution (0.5 mg/mL) by drop-casting and dried at room temperature. Second, 10 μL of 5% GA solution was dropped onto the surface of the electrode to activate the modified electrode, and kept at 37 °C for 30 min. Ten microliters of 0.01 mg/mL anti-CEA solution (10 mM PBS, PH 7.4) was dropped onto the activated electrode and incubated at 4 °C for 12 h, after which it was washed with DI water. Ten microliters of 1 wt % BSA as a blocking reagent was dropped onto the electrode surface for 1 h at 37 °C to eliminate nonspecific binding sites. Last, the resulting electrode was incubated with 10 μL of different concentrations of CEA

at 37 °C for 1 h and rinsed with PBS (10 mM, pH 7.4). All fabrication steps of the electrochemical biosensor are shown in Scheme 1.

Scheme 1. Fabricating Steps of the Electrochemical Immunosensor
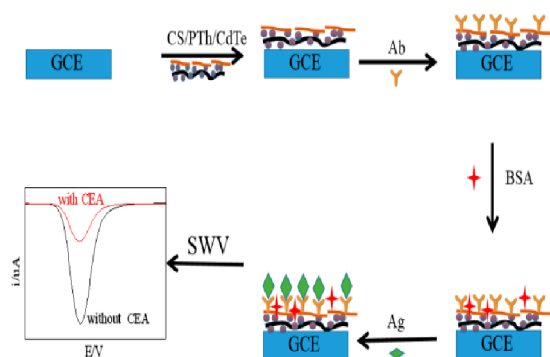
2.6. Electrochemical Detection.
All electrochemical measurements were conducted at room temperature with BSA/Ab/CS/PTh/CdTe/GCE as the working electrode, a platinum wire electrode as the counter electrode, and a saturated electrode as the reference electrode.

Electrochemical impedance spectroscopy (EIS) was used to study the preparation of immunosensor within 5.0 mM of $K_3Fe(CN)_6/K_4Fe(CN)_6$ and 0.1 M of KCl from 0.01 Hz to 100 kHz with an amplitude of 5 mV. The electrode was incubated by a series of CEA samples (10 μL) with various concentrations at 37 °C for 60 min. The electrochemical measurement was carried out in a mixture of 0.1 M PBS (pH 7.0), 0.1 M KCl, and 20 mM $K_4Fe(CN)_6$ with the scanning potential ranging from −0.2 to 0.8 V, an amplitude of 0.05 V, a pulse width of 0.05 s, and a quiet time of 2 s to obtain the SWV signal.

3. RESULTS AND DISCUSSION

3.1. Characterization of CS/PTh/CdTe Nanocomposites.
The morphology of the synthesized CS/PTh/CdTe nanocomposites was characterized by SEM and TEM. The nanocomposites are of flocculent wool-like morphology (Figure 1A), with CdTe QDs evenly distributed on the surface of CS/PTh (Figure 1B), providing more active sites for the attachment of antibodies and subsequent improvement of the electronic transfer rate. The cubic phase of CdTe had an interplanar spacing of $d = 0.371$ nm, which is presented in Figure 1B (inset). The FTIR spectra of CdTe QDs (blue), PTh/CdTe (red), and CS/PTh/CdTe (black) are all characterized and presented in Figure 1C. As presented, characteristic peaks at 3430 and 1134 cm^{-1}, attributed to the stretching vibrations and bending vibrations of O−H, respectively, are all observed.[7,46] Two main characteristic peaks at 1620 and 1400 cm^{-1}, ascribed to the antisymmetrical and symmetric vibrations of carboxyl, respectively, further prove that electrodes are successfully modified by chitosan.[46] The characteristic peak of the amino group at 1560 cm^{-1} and the C−N bending vibrations at 1405 cm^{-1} indicate successful capping of L-Cys. The peak at 1085 cm^{-1} ascribed to the vibration of −C−O−C− further demonstrates successful modification of the electrode with chitosan.[39]

An XPS measurement of CS/PTh/CdTe is performed and shown in Figure 1D−G. The characteristic peaks of Cd 3d$_{3/2}$ at

412.0 eV and Cd 3d$_{5/2}$ at 405.1 eV contribute to the binding energy of Cd (II+) (Figure 1D). The Te 3d$_{3/2}$ peak at 583.0 eV and the Te 3d$_{5/2}$ peak at 572.5 eV are attributed to the binding energy of Te (II−) (Figure 1E). The shoulder peak on the high-binding energy side of Te peak confirms the presence of Te (IV+) in the form of CdTe nanocrystals.[47] The peak at 531.5 eV in the O 1s spectrum is attributed to COO$^-$ or tellurium oxides (Figure 1F). The peak at 162.5 eV in the S 2p spectrum (Figure 1G) shows sulfur in the form of C−S−C or Cd−S−C. Meanwhile, the peak at 168.8 eV suggests the existence of sulfur oxides.[48,49] The XPS spectrum reveals the presence of the main elements in the CS/PTh/CdTe nanocomposite sample (Figure 1H).

3.2. Electrochemical Behavior of the Electrodes.
EIS analysis is evoked to evaluate the interfacial characteristic of the modified electrode.[50] According to the Nyquist plots (Figure 2A), the resistance of bare electrode, CdTe, and polythiophene ranks as bare electrode < polythiophene < CdTe. The modification of the bare electrode with CdTe leads to an increase in the polarization resistance of the modified electrode (curve d); however, doping of PTh and CS greatly improves the conductivity of the modified electrode, which is beneficial to amplify the signal of electrochemical analysis.

To explore the reliability of the electrode, EIS analysis of the electrode at different modification stages is also conducted and presented in Figure 2B. The immobilization of CS/PTh/CdTe on the bare GCE electrode increases the resistance of the electrode possibly due to the electrostatic repulsion of $[Fe(CN)_6]^{3-/4-}$ via the negatively charged carboxy group of CS/PTh/CdTe (Figure 2B, curves a). The immobilization of antibody and BSA on electrode increases the electro-resistance of the electrode because of the insulation of the protein layer (Figure 2B, curves b,c). The modification of the electrode with antigen further retards the interfacial electron transfer on the surface of the electrode (Figure 2B, curves d). The EIS results confirm that the immunosensor is successfully fabricated.

3.3. Electrochemical Properties of the CS/PTh/CdTe Nanocomposites.
The SWVs of GCE, CS/PTh/CdTe/GCE, Ab/CS/PTh/CdTe/GCE, BSA/Ab/CS/PTh/CdTe/GCE, and Ag/BSA/Ab/CS/PTh/CdTe are recorded and shown in Figure 3. As demonstrated, the current signal of the bare GCE electrode in PBS (0.1 M, pH 7.0) is near zero. However, there is a significant current signal of bare GCE in PBS with $K_4Fe(CN)_6$ at 0.25 V (curve b), due to the redox reaction of $Fe(CN)_6^{4-}$ on the surface of the electrode. When the GCE electrode is modified with CS/PTh/CdTe nanocomposite, a small peak at 0.29 V of CS/PTh/CdTe-modified GCE in PBS buffer solution appeared due to the oxidation of CdTe.[51] The current peaks of $K_4Fe(CN)_6$ and CS/PTh/CdTe disappear with an increase of $K_4Fe(CN)_6$ in PBS buffer solution, and a greater current peak presents at 0.189 V (curve d). It is supposed that the catalytic oxidation of $K_4Fe(CN)_6$ could facilitate the oxidation of CS/PTh/CdTe nanocomposites on the GCE electrode.[52] The electron transfer on the surface of the electrode leads to an increase of the peak current and a negative shift of the peak potential. However, contact between $K_4Fe(CN)_6$ and CS/PTh/CdTe is unavoidably hindered when the antibody and BSA incubate on the surface of the electrode, subsequently resulting in a decrease of the current (curves e,f). The specific recognition of antigen−antibody on the surface of the electrode makes the antigen (Ag) further incubate on the surface of the electrode, hindering the contact between $K_4Fe(CN)_6$ and CS/PTh/CdTe. There-
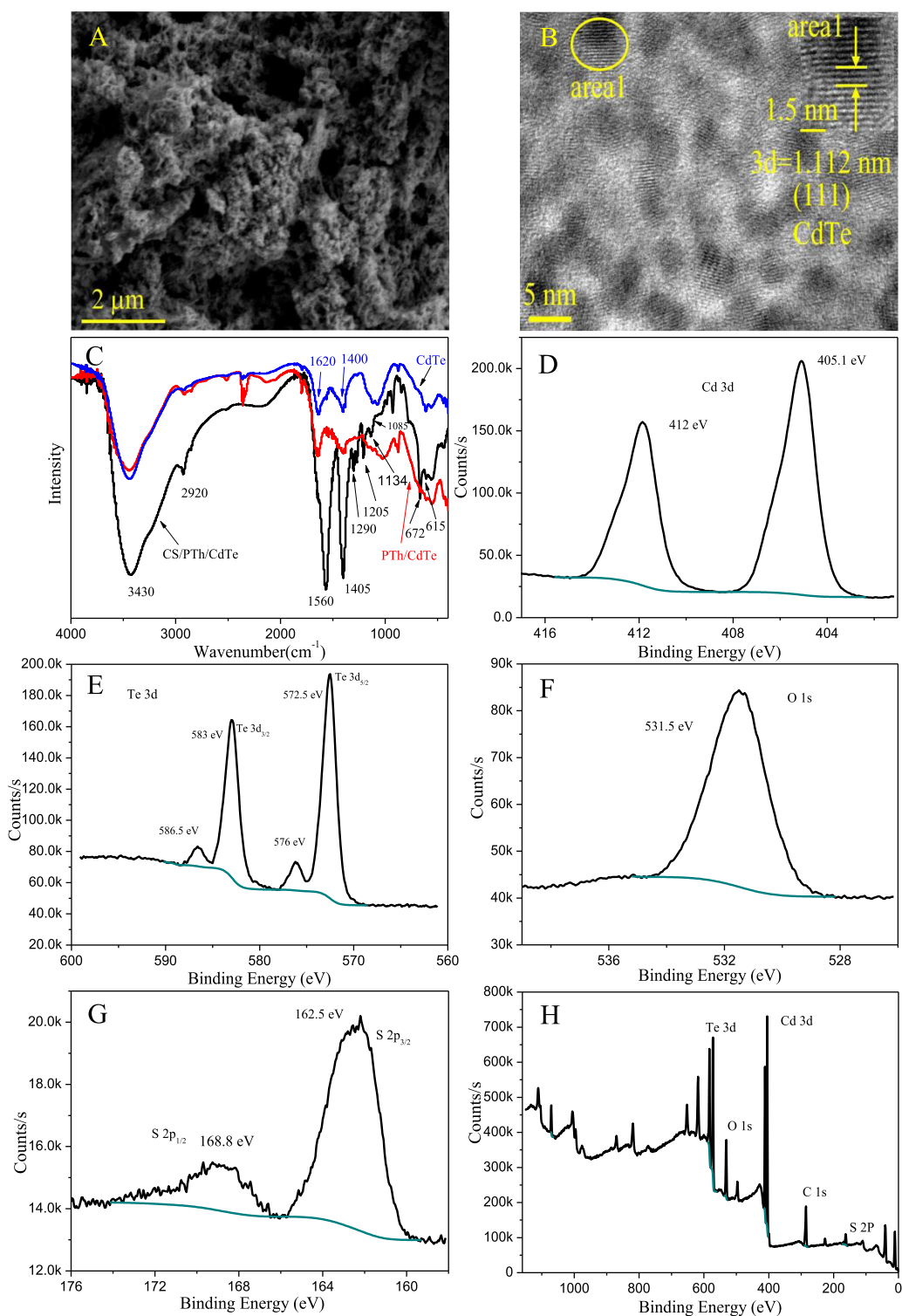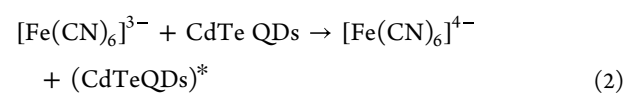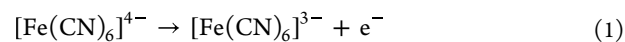
Figure 1. Measurement results of the products: (A) SEM image of CS/PTh/CdTe; (B) TEM image of CS/PTh/CdTe; and (C) FTIR absorption spectra. XPS spectra of the CS/PTh/CdTe product: (D) Cd 3d core level spectrum; (E) Te 3d core level spectrum; (F) O 1s core level spectrum; (G) S 2p core level spectrum; and (H) survey spectrum.

fore, a significant decrease of current is observed due to the reduction of the catalytic effect (curve g), which can be consequently used as an indicator for detecting CEA antigens. The mechanisms of detection of CEA in 0.1 M PBS with $K_4Fe(CN)_6$ solution via the BSA/Ab/CS/PTh/CdTe/GCE and Ag/BSA/Ab/CS/PTh/CdTe/GCE electrodes are illustrated in Scheme 2.

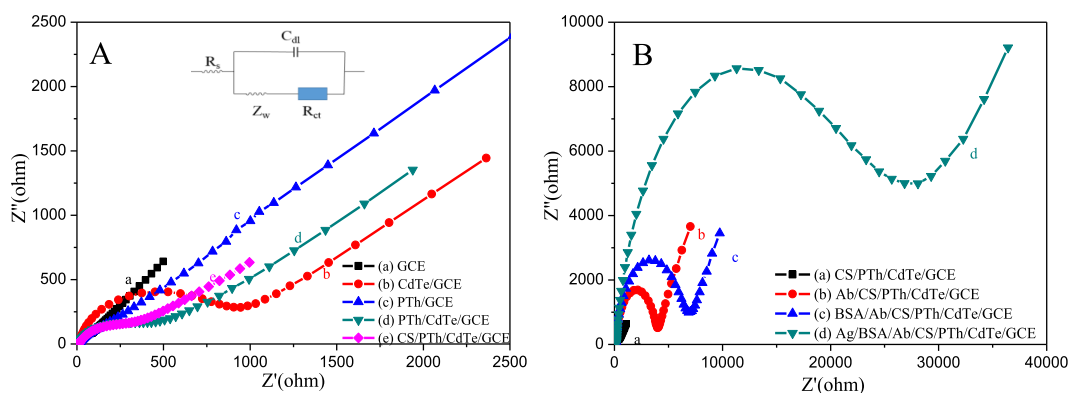The electron transfer mechanism could be expressed simply as follows:

$$[Fe(CN)_6]^{4-} \rightarrow [Fe(CN)_6]^{3-} + e^- \qquad (1)$$

$$[Fe(CN)_6]^{3-} + CdTe\ QDs \rightarrow [Fe(CN)_6]^{4-} + (CdTeQDs)^* \qquad (2)$$

Figure 2. EIS of (A) the following materials: (a) bare GCE electrode; (b) CdTe/GCE electrode; (c) PTh/GCE electrode; (d) PTh/CdTe/GCE electrode; and (e) CS/PTh/CdTe/GCE electrode. EIS of (B) the stepwise biosensor fabrication: (a) CS/PTh/CdTe/GCE electrode; (b) Ab/CS/PTh/CdTe/GCE electrode; (c) BSA/Ab/CS/PTh/CdTe/GCE electrode; and (d) Ag/BSA/Ab/CS/PTh/CdTe/GCE electrode. EIS for the stepwise biosensor fabrication was measured in the frequency range between 0.01 Hz and 100 kHz with an amplitude of 5 mV; the concentration of CEA was 10 ng/mL. Inset: Equivalent circuits.
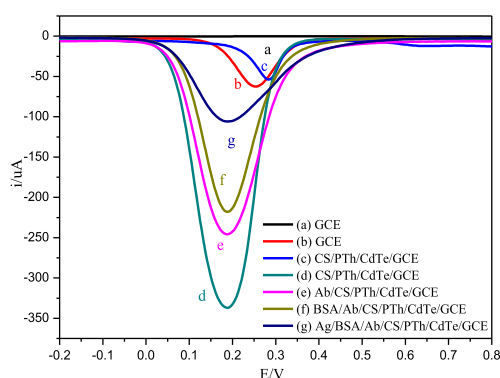

Figure 3. SWV curve of (a) bare GCE electrode in PBS; (b) bare GCE electrode in PBS with $K_4Fe(CN)_6$; (c) CS/PTh/CdTe/GCE electrode in PBS; (d) CS/PTh/CdTe/GCE in PBS with $K_4Fe(CN)_6$; (e) Ab/CS/PTh/CdTe/GCE in PBS with $K_4Fe(CN)_6$; (f) BSA/Ab/CS/PTh/CdTe/GCE in PBS with $K_4Fe(CN)_6$; and (g) Ag/BSA/Ab/CS/PTh/CdTe/GCE in PBS with $K_4Fe(CN)_6$. The SWV curve was obtained in different components of PBS (0.1 M, pH 7.0, with or without 20 mM of $Fe(CN)_6^{4-}$); the concentration of CEA is 10 ng/mL.

$$(CdTe\ QDs)^* + H_2O \rightarrow CdTeO_3 + H^+ + e^- \quad (3)$$

To verify the above electron transfer mechanism (formulas 1−3),[52] in situ infrared spectro-electrochemical studies have been carried out in the thin-layer electrochemical cell.[53] As shown in Figure 4A, the CV curves of GCE, CS/PTh/GCE, and CS/PTh/CdTe/GCE in 0.1 M PBS solution with 20 mM $K_4Fe(CN)_6$ (pH 7.0) in the scanning range of −0.2−1.0 V and the corresponding IR 3D spectra are recorded simultaneously. In comparison, bare GCE and PTh/CS/GCE have good reversible redox peaks (curves a and b), while the oxidation current of CS/PTh/CdTe/GCE is larger than its reduction current (curve c).

According to the in situ FT-IR spectra, there are two absorption peaks observed in the spectra of bare GCE (Figure 4B) and CS/PTh/GCE (Figure 4C) in the wavenumber range of 1000−2500 cm^{-1} (corresponding to the electrochemical process from −0.2 to 1.0 V) with spectra gathered at −0.2 V as the reference spectrum. There are two types of IR peaks with a negative band at 2036 cm^{-1} assigned to the consumption of $Fe(CN)_6^{4-}$, and an upward peak at 2115 cm^{-1} attributed to the formation of the $Fe(CN)_6^{3-}$ observed.[53] The corresponding

Scheme 2. Reaction Process Mechanism of the BSA/Ab/CS/PTh/CdTe/GCE and Ag/BSA/Ab/CS/PTh/CdTe/GCE Electrodes in 0.1 M PBS with $K_4Fe(CN)_6$ Solution[a]
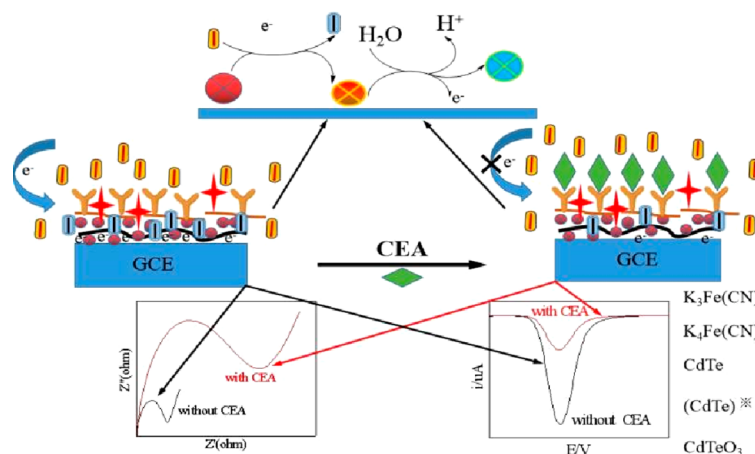
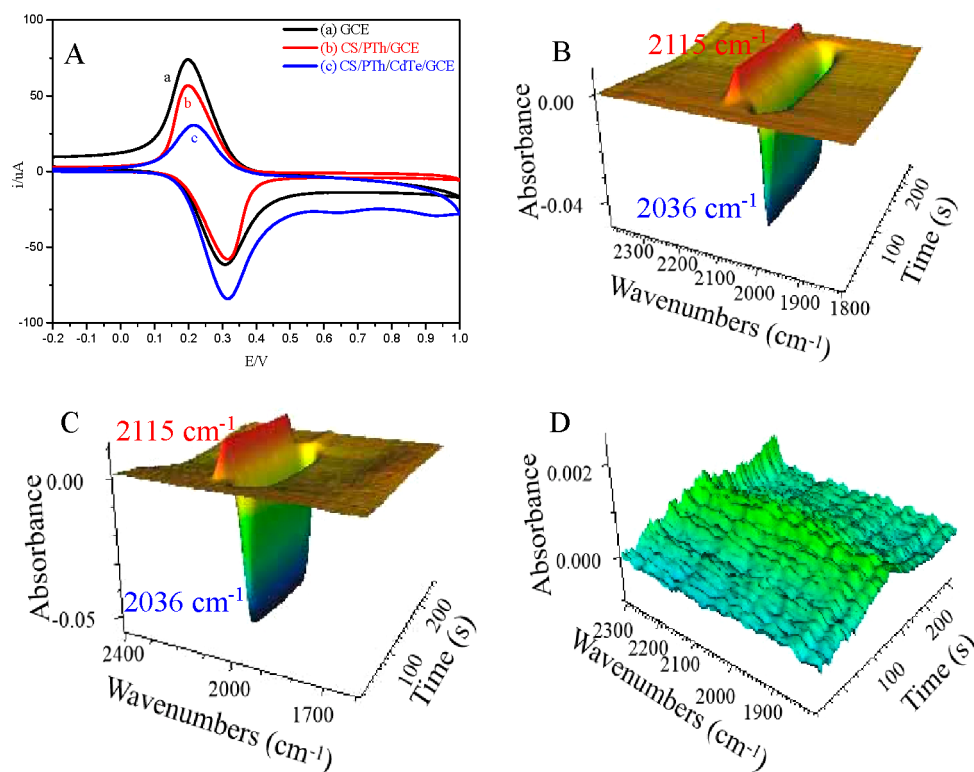[a]The concentration of CEA is 10 ng/mL.

Figure 4. (A) Thin-layer CV of (a) GCE, (b) CS/PTh/GCE, and (c) CS/PTh/CdTe/GCE in 0.1 M PBS containing 20 mM $K_4Fe(CN)_6$; and the corresponding 3D spectra of (B) GCE, (C) GCE/PTh/CS, and (D) CS/PTh/CdTe/GCE. Potential scan rate: 10 mV/s.
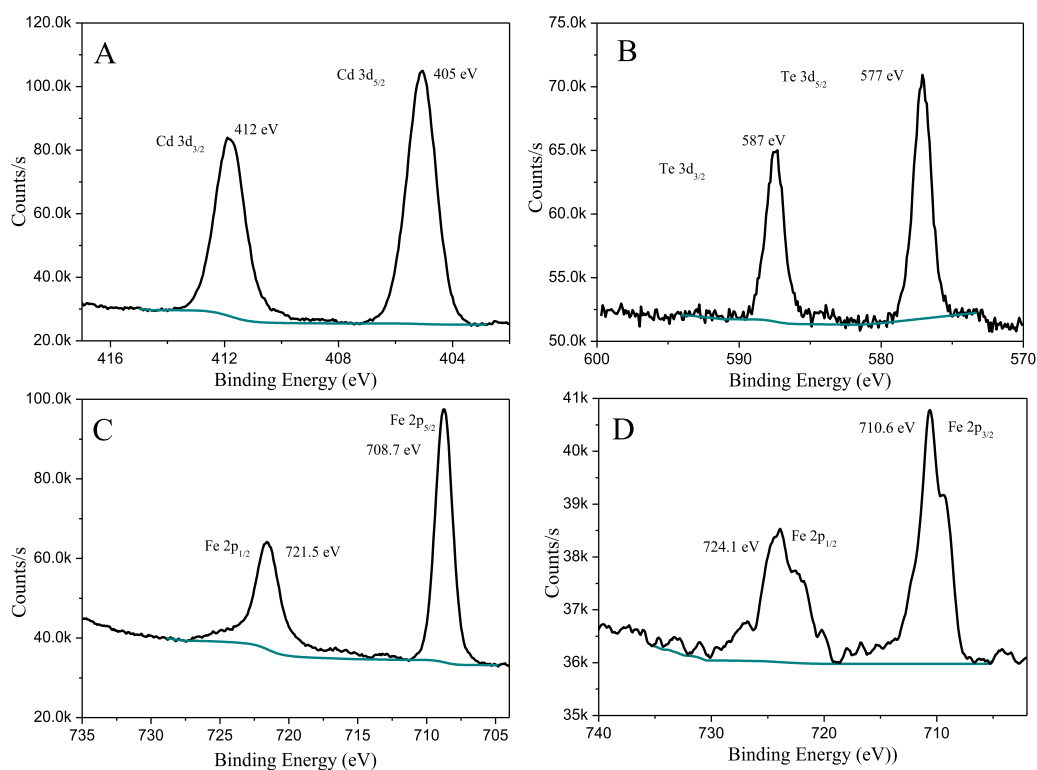

Figure 5. XPS spectra of the postreaction product: (A) Cd 3d core level spectrum; (B) Te 3d core level spectrum; (C) Fe 2p core level spectrum of $K_4Fe(CN)_6$ after it reacts with CS/PTh/CdTe; and (D) Fe 2p core level spectrum of $K_4Fe(CN)_6$ after it reacts with CS/PTh.

3D spectra of CS/PTh/CdTe/GCE are shown in Figure 4D. No IR absorption peak at 2036 and 2115 cm^{-1} is observed because $K_3Fe(CN)_6$ generated by electrochemical oxidation is rapidly reduced to $K_4Fe(CN)_6$; that is, the reaction shown in formula 2 occurred.

To reveal the surface composition and elemental valence of the electrochemical products of $K_4[Fe(CN)_6]$ attached on the
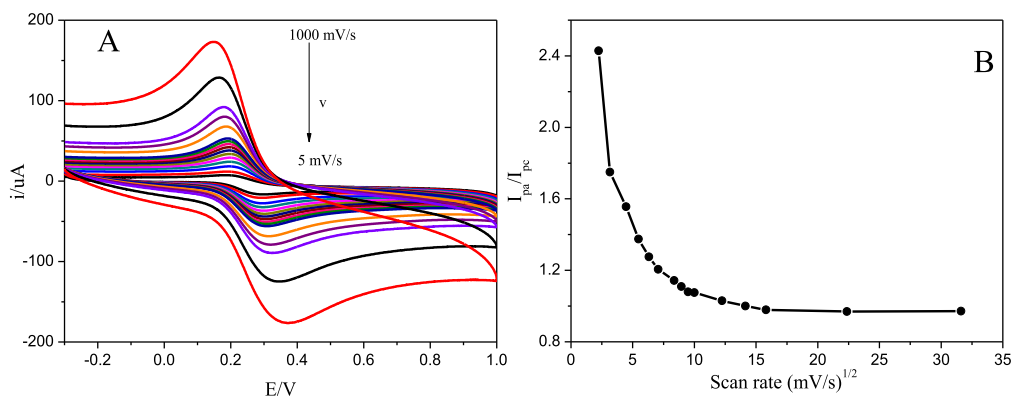
Figure 6. (A) CV of CS/PTh/CdTe in 0.1 mM PBS contain 20 mM $K_4Fe(CN)_6$ at different scanning rates from 5 to 1000 mV/s; and (B) the ratio of I_{pa}/I_{pc} at different scanning rates.

surface of CS/PTh/CdTe or CS/PTh, XPS analysis of the pre- and postelectrochemical reaction is studied and shown in Figure 5. The characteristic peaks of Cd $3d_{3/2}$ at 412.0 eV, Cd $3d_{5/2}$ at 405.0 eV (Figure 5A), Te $3d_{3/2}$ peak at 587.0 eV, and Te $3d_{5/2}$ at 577.0 eV (Figure 5B) correspond to the binding energy of Cd (II+) and Te (IV+), respectively, indicating that Cd (II+) remains unchanged, while all of the Te (II−) in CdTe is oxidized to Te (IV+) according to the current signal caused by the change of valence of tellurium.[54] The XPS spectrum of Fe 2p after the electrochemical reaction of CS/PTh/CdTe is shown in Figure 5C. Two strong peaks at 721.5 and 708.7 eV are comparable to those of $K_4Fe(CN)_6$, indicating that there is no change of electrolyte during the oxidation process.[55,56] When the above experiment is repeated with CS/PTh electrode instead, an Fe $2p_{3/2}$ peak at 710.6 eV and an Fe $2p_{1/2}$ peak at 724.1 eV corresponding to the binding energy of Fe (III+) are observed because Fe (II+) is oxidized to Fe (III+) after the electrochemical reaction (Figure 5D).[57] The results of XPS analysis are consistent with the results of IR spectroelectrochemistry.

The CV curves of CS/PTh/CdTe in a mixture of 0.1 mM PBS and 20 mM $K_4Fe(CN)_6$ are scanned at a rate of 5−1000 mV/s. The CV curves show a good redox couple with a gradual increase of current intensity with the increase of scanning rate. Meanwhile, a larger oxidation current (I_{pa}) than the reduction current (I_{pc}) with $I_{pa}/I_{pc} \geq 1$ is demonstrated (Figure 6A), suggesting that $K_4Fe(CN)_6$ catalyzes the electrochemical reaction of CS/PTh/CdTe (Figure 6B).

The influence of $K_4Fe(CN)_6$ concentration on the electro-chemical intensity is also investigated. As shown in Figure 7, the electrochemical signals of the GCE electrode and CS/PTh/GCE electrode increase with the increase of $K_4Fe(CN)_6$ concentration. Moreover, the increased amplitude of the electrochemical signals of the GCE electrode is larger than that of the CS/PTh/GCE electrode due to hindered electron transfer by CS/PTh. The electrochemical intensity of the CS/PTh/CdTe/GCE electrode remains constant when the concentration of $K_4Fe(CN)_6$ is higher than 20 mM. Therefore, $K_4Fe(CN)_6$ is a catalyst of the electrochemical oxidation of CdTe rather than a probe.

3.4. Condition Optimization. To improve the CEA detection sensitivity of the immunosensor, the concentrations of $K_4Fe(CN)_6$ and CS/PTh/CdTe, the pH of PBS, the incubation temperature of antigen, and the incubation time are optimized. The optimization of the experimental conditions was shown in Figures S1A−S1E.
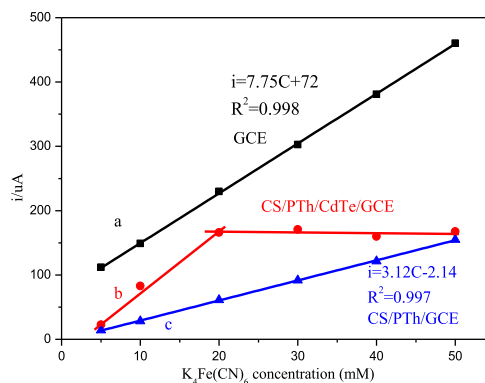

Figure 7. Corresponding calibration curve of (a) GCE, (b) CS/PTh/CdTe/GCE, and (c) CS/PTh/GCE in 0.1 M PBS containing different concentrations of $K_4Fe(CN)_6$ (5−50 mM, respectively).

3.5. Performance of the Biosensor for the Detection of CEA. The detection of CEA via a fabricated CS/PTh/CdTe/GCE immunosensor under optimal reactions is conducted. As shown in Figure 8B, a linear relationship between the SWV signal intensity and the logarithm of CEA concentration (log C) is observed with a linear equation (R^2 = 0.9983) listed as follows: $I = -18.98 \times \log C_{CEA} + 120.3$, where I (μA) is the current signal and C_{CEA} (ng/mL) is the concentration of CEA. Noteworthy, the SWV signal decreases with an increase of CEA concentration due to the hindered transfer of electrons caused by the formation of an immunocomplex (Figure 8A). The results indicate that CEA ranging from 0.0001 to 10000 ng/mL can be quantitatively detected with a limit of 40 fg/mL (S/N = 3).

As compared to previous studies shown in Table 1, the CS/PTh/CdTe/GCE immunosensor fabricated in this work has a relatively lower detection limit and wider linear range. Moreover, the average recovery efficiency of six CEA detection tests with different concentrations in the normal serum samples ranged from 99.8−105% with a relative standard deviation (RSD) of 4.1−5.2% (Table 2), confirming that the proposed electrochemical biosensor is an ultrasensitive tool for the determination of CEA in biological samples with remarkable reproducibility. The inter-assay and intra-assay repeatability of the electrochemical biosensor of the detection tests results is shown in Table S1.

To further study the selectivity of the immunosensor, the detection of CEA with target and nontarget by adding IL-6 (100 ng/mL), MUC1 (100 ng/mL), L-ascorbic acid (100 ng/
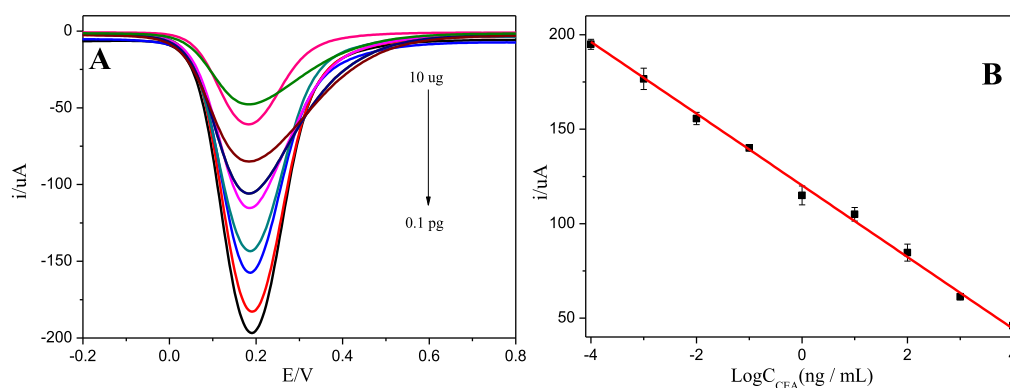
Figure 8. (A) Square wave voltammetry response and (B) the corresponding calibration curve of the biosensor for the CEA assay (from 0.0001 to 10 000 ng/mL, respectively).

Table 1. Comparison of Different Sensing Methods on the Detection of CEA

electrode/materials	method	linear range (ng/mL)	detection limit	ref
CdTe/RGO-AuNPs	PEC	0.001−2.0	0.47 pg/mL	58
CdTe	CVG-AFS/ICP-MS	0.5−20	0.2 ng/mL	59
Mn:ZnCdS@ZnS/CdTe	FL	0.0001−10	65 fg/mL	60
NaYF$_4$:Yb,Er/Ag$_2$S	PEC	0.005−5	1.9 pg/mL	61
H$_2$O and CaO	thermometers	0.00781−0.5	0.6 pg/mL	62
AuNPs/MoS$_2$	colorimetric	0.005−10	0.5 pg/mL	63
AuNPs	colorimetric	10−120	3 ng/mL	16
BIQ-1	fluorescent	0−200	0.2 ng/mL	15
CS/PTh/CdTe	electrochemistry	0.0001−10000	40 fg/mL	this work

Table 2. Recovery Tests for CEA Samples Using the Proposed Method ($n = 6$)

samples	add (pg)	found (pg)	rate of recovery (%)	RSD (%)
1	5.000	5.200	104.0	5.2
2	50.00	52.60	105.0	4.1
3	500.0	499.0	99.80	4.6
4	5000	5087	102.0	4.7

mL), and a mixture (100 ng/mL of IL-6, 100 ng/mL of MUC1, 100 ng/mL of L-ascorbic acid, and 10 ng/mL of CEA) was depicted in Figure 9. The biosensor is proved to be highly selective for the detection of CEA with negligible changes
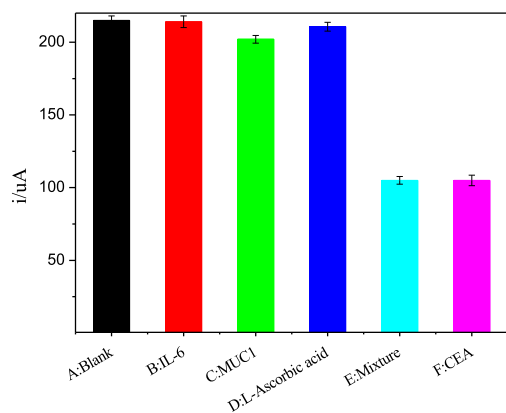

Figure 9. Selectivity of the proposed electrochemical biosensor with different targets: (A) blank; (B) 100 ng/mL of IL-6; (C) 100 ng/mL of MUC1; (D) 100 ng/mL of L-ascorbic acid; (E) a mixture (containing 100 ng/mL of IL-6, 100 ng/mL of MUC1, 100 ng/mL of L-ascorbic acid, and 10 ng/mL of CEA); and (F) 10 ng/mL of CEA.

caused by the other interfering biomolecules. The stability of the biosensor for the detection of CEA was evaluated at 4 °C for one month. The results show that the immunosensor exhibited good stability without a significant change in the SWV signal.

4. CONCLUSIONS

In this work, CS/PTh/CdTe nanocomposites were directly synthesized by the one-step method and were linked with previously functionalized anti-CEA via the covalent bond reaction to construct the sandwich-like immunosensor for ultrasensitive detection of CEA. The immunosensor had a wider linear concentration range of 0.0001−10 000 ng/mL with a detection limit of 40 fg/mL (S/N = 3), as well as favorable reproducibility, durable stability, and satisfactory selectivity and sensitivity due to that the electrochemical oxidation products of $K_4Fe(CN)_6$ can directly oxidize CdTe from a low energy state to a high energy state (CdTe)*, which facilitates electron transfer at the electrode with an amplified signal of biosensor during CEA detection. Because of its simple preparation and high sensitivity, this biosensor holds great promise for the clinical detection of tumors.

■ ASSOCIATED CONTENT

ⓢ Supporting Information

The Supporting Information is available free of charge at https://pubs.acs.org/doi/10.1021/acsomega.2c05950.

Influence of (A) the concentration of CS/PTh/CdTe, (B) the concentration of $K_4Fe(CN)_6$, (C) the pH value, (D) the incubation time for CEA, and (E) the incubation temperature of CEA; and the inter-assay and intra-assay repeatability of the electrochemical biosensor (Table S1) (PDF)

■ AUTHOR INFORMATION

Corresponding Author

Baokang Jin − *Department of Chemistry, Anhui University, Hefei 230601, China;* ⊙ orcid.org/0000-0002-1719-3975; Email: bkjinhf@aliyun.com

Authors

Jiajia Wang − *Department of Chemistry, Anhui University, Hefei 230601, China*

Xin Hua − *Department of Chemistry, Anhui University, Hefei 230601, China*

Complete contact information is available at:
https://pubs.acs.org/10.1021/acsomega.2c05950

Notes

The authors declare no competing financial interest.

■ REFERENCES

(1) Melo, M. I. A. D.; Correa, C. R.; Cunha, P. D. S.; Góes, A. M. D.; Gomes, D. A.; Andrade, A. S. R. D. DNA aptamers selection for carcinoembryonic antigen (CEA). *Bioorg. Med. Chem. Lett.* **2020**, *30*, 127278−127286.

(2) Molin, R.; Barak, V.; Dalen, A. V.; Duffy, M. J.; Einarsson, R.; Gion, M.; Goike, H.; Lamerz, R.; Nap, M.; Sölétormos, G.; Stieber, P. Tumor Markers in Breast Cancer- European Group on Tumor Markers, Recommendations. *Tumor Biol.* **2005**, *26*, 281−293.

(3) Juweid, M.; Sharkey, R. M.; Swayne, L. C.; Goldenberg, D. M.; Morristown, B. Improved selection of patients for reoperation for medullary thyroid cancer by imaging with radiolabeled anticarcinoembryonic antigen antibodies. *Surgery* **1997**, *122*, 1156−1165.

(4) Malekshahi, Z. V.; Goradel, N. H.; Khomartash, M. S.; kadkhodazadeh, M.; Maleksabet, A.; Kardar, G. A.; Negahdari, B. CEA Plasmid as Therapeutic DNA Vaccination against Colorectal Cancer. *Iran. J. Immunol.* **2019**, *16*, 235−245.

(5) Meng, Q. C.; Shi, S.; Liang, C.; Liang, D. K.; Xu, W. Y.; Ji, S. R.; Zhang, B.; Ni, Q. X.; Xu, J.; Yu, X. J. Diagnostic and prognostic value of carcinoembryonic antigen in pancreatic cancer: a systematic review and meta-analysis. *Onco Targets Ther.* **2017**, *10*, 4591−4598.

(6) Pei, F. B.; Wang, P.; Ma, E. H.; Yu, H. X.; Gao, C. X.; Yin, H. H.; Li, Y. Y.; Liu, Q.; Dong, Y. H. A sandwich-type amperometric immunosensor fabricated by Au@Pd NDs/ Fe²⁺-CS/PPy NTs and Au NPs/NH₂-GS to detect CEA sensitively via two detection methods. *Biosens. Bioelectron.* **2018**, *122*, 231−238.

(7) Liu, Q.; Yang, Y.; Liu, X. P.; Wei, Y. P.; Mao, C. J.; Chen, J. S.; Niu, H. L.; Song, J. M.; Zhang, S. Y.; Jin, B. K.; Jiang, M. A facile in situ synthesis of MIL-101-CdSe nanocomposites forultrasensitive electrochemiluminescence detection of carcinoembryonic antigen. *Sensor. Actuat. B* **2017**, *242*, 1073−1078.

(8) Zheng, J. Y.; Di, Y.; Gao, L. M.; Kong, X. L.; Zheng, Y.; Han, J. L.; Wang, J. D. Construction of fluorescent biosensing system based on DNA templated quantum dots-graphene oxide interactions for detecting carcinoembryonic antigen. *Mater. Technol.* **2022**, *37*, 2116.

(9) Qiu, Z. L.; Shu, J.; Liu, J. F.; Tang, D. P. Dual-Channel Photoelectrochemical Ratiometric Aptasensor with up-Converting Nanocrystals Using Spatial-Resolved Technique on Homemade 3D Printed Device. *Anal. Chem.* **2019**, *91*, 1260−1268.

(10) Li, X. Y.; Wang, R. Y.; Zhang, X. L. Electrochemiluminescence immunoassay at a nanoporous gold leaf electrode and using CdTe quantun dots as labels. *Microchim. Acta* **2011**, *172*, 285−290.

(11) Yang, M. L.; Chen, Y.; Xiang, Y.; Yuan, R.; Chai, Y. Q. In situ energy transfer quenching of quantum dot electrochemi- luminescence for sensitive detection of cancer biomarkers. *Biosens. Bioelectron.* **2013**, *50*, 393−398.

(12) Jie, G. F.; Liu, P.; Zhang, S. S. Highly enhanced electrochemiluminescence of novel gold/silica/CdSe-CdS nanostructures for ultrasensitive immunoassay of protein tumor marker. *Chem. Commun.* **2010**, *46*, 1323−1325.

(13) Liu, Y. M.; Yue, H. Y.; Tian, W.; Chen, Y. H.; Li, F. R. Quantification of Carcinoembryonic Antigen by Capillary Electrophoresis-Chemiluminescence, Detection using Internal Standard Method. *Anal. Lett.* **2009**, *42*, 45−57.

(14) Chon, H.; Lee, S.; Son, S. W.; Oh, C. H.; Choo, J. Highly Sensitive Immunoassay of Lung Cancer Marker Carcinoembryonic Antigen Using Surface-Enhanced Raman Scattering of Hollow Gold Nanospheres. *Anal. Chem.* **2009**, *81*, 3029−3034.

(15) Lee, J. S.; Song, I. H.; Warkad, S. D.; Yeom, G. S.; Nimse, S. B. An abiotic fluorescent probe for the detection and quantification of carcinoembryonic antigen. *Bioorg. Chem.* **2022**, *119*, 105490.

(16) Luo, C.; Wen, W.; Lin, F. G.; Zhang, X. H.; Gu, H. H.; Wang, S. F. Simplified aptamer-based colorimetric method using unmodified gold nanoparticles for the detection of carcinoma embryonic antigen. *RSC Adv.* **2015**, *5*, 10994−10999.

(17) Zhu, Y. L.; Lian, Y. M.; Wang, J. K.; Chen, Z. P.; Yu, R. Q. Ultrasensitive detection of protein biomarkers by MALDI-TOF mass spectrometry based on ZnFe₂O₄ nanoparticles and mass tagging signal amplification. *Talanta* **2021**, *224*, 121848−121856.

(18) Su, F. Y.; Murayama, K.; Xu, C. Y.; Taya, M.; Nishimura, S. I.; Shinohara, Y. Detection of carcinoembryonic antigens using a surface plasmon resonance biosensor. *Sensors* **2008**, *8*, 4282−4295.

(19) Qiu, Y. C.; Deng, D.; Deng, Q. W.; Wu, P.; Zhang, H.; Cai, C. X. Synthesis of magnetic Fe₃O₄-Au hybrids for sensitive SERS detection of cancer cells at low abundance. *J. Mater. Chem. B* **2015**, *3*, 4487−4495.

(20) Gu, X. F.; She, Z.; Ma, T. X.; Tian, S. Electrochemical detection of carcinoem- bryonic antigen. *Biosens. Bioelectron.* **2018**, *102*, 610−616.

(21) Chen, Y.; Wang, A. J.; Yuan, P. X.; Luo, X. L.; Xue, Y. D.; Feng, J. J. Three dimensional sea-urchin-like PdAuCu nanocrystals/ferrocene-grafted-polylysine as an efficient probe to amplify the electrochemical signals for ultrasensitive immunoassay of carcinoembryonic antigen. *Biosens. Bioelectron.* **2019**, *132*, 294−301.

(22) Feng, Y. G.; He, J. W.; Jiang, L. Y.; Chen, D. N.; Feng, J. J. Novel sandwich-typed electrochemical immunosensing of C-reactive protein using multiply twinned AuPtRh nanobead chains and nitrogen-rich porous carbon nanospheres decorated with Au nanoparticles. *Sensor. Actuat. B-Chem.* **2022**, *358*, 131518.

(23) Tang, H.; Chen, J. H.; Nie, L. H.; Kuang, Y. F.; Yao, S. Z. A label-free electrochemical immunoassay for carcinoem- bryonic antigen (CEA) based on gold nanoparticles (AuNPs) and nonconductive polymer film. *Biosens. Bioelectron.* **2007**, *22*, 1061−1067.

(24) Yu, Z. Z.; Cai, G. N.; Liu, X. L.; Tang, D. P. Pressure-Based Biosensor Integrated with a Flexible Pressure Sensor and an Electrochromic Device for Visual Detection. *Anal. Chem.* **2021**, *93*, 2916−2925.

(25) Qiu, Z. L.; Shu, J.; Tang, D. P. Bioresponsive Release System for Visual Fluorescence Detection of Carcinoembryonic Antigen from Mesoporous Silica Nanocontainers Mediated Optical Color on Quantum Dot-Enzyme-Impregnated Paper. *Anal. Chem.* **2017**, *89*, 5152−5160.

(26) Zhang, K. Y.; Lv, S. Z.; Zhou, Q.; Tang, D. P. CoOOH nanosheets-coated g-C₃N₄/CuInS₂ nanohybrids for photoelectrochemical biosensor of carcinoembryonic antigen coupling hybridization chain reaction with etching reaction. *Sensor. Actuat. B-Chem.* **2020**, *307*, 127631.

(27) Yu, Z. Z.; Tang, Y.; Cai, G. N.; Ren, R. R.; Tang, D. P. Paper Electrode-Based Flexible Pressure Sensor for Point-of-Care Immunoassay with Digital Multimeter. *Anal. Chem.* **2019**, *91*, 1222−1226.

(28) Feng, T. T.; Qiao, X. W.; Wang, H. N.; Sun, Z.; Qi, Y.; Hong, C. L. An electrochemical immunosensor for simultaneous point-of-

care cancer markers based on the host-guest inclusion of b-cyclodextrin-graphene oxide. *J. Mater. Chem. B* **2016**, *4*, 990−996.

(29) Shu, H. W.; Wen, W.; Xiong, H. Y.; Zhang, X. H.; Wang, S. F. Novel electrochemical aptamer biosensor based on gold nanoparticles signal amplification for the detection of carcinoembryonic antigen. *Electrochem. Commun.* **2013**, *37*, 15−19.

(30) Wang, Y. G.; Wang, Y. L.; Wu, D.; Ma, H. M.; Zhang, Y.; Fan, D. W.; Pang, X. H.; Du, B.; Wei, Q. Label-free electrochemical immunosensor based on flower-like Ag/MoS₂/rGO nanocomposites for ultrasensitive detection of carcinoembryonic antigen. *Sensor. Actuat. B* **2018**, *255*, 125−132.

(31) Yalla, R.; Nayak, K. P.; Hakuta, K. Fluorescence photon measurements from single quantum dots on an optical nanofiber. *Opt. Express* **2012**, *20*, 2932−2941.

(32) Gromova, Y. A.; Orlova, A. O.; Maslov, V. G.; Fedorov, A. V.; Baranov, A. V. Fluorescence energy transfer in quantum dot/azodye complexes in polymer track membranes. *Nanoscale Res. Lett.* **2013**, *8*, 452−457.

(33) Ding, M. L.; Wang, K.; Fang, M.; Zhu, W. J.; Du, L. C.; Li, C. MPA-CdTe quantum dots as "on-off-on" sensitive fluorescence probe to detect ascorbic acid via redox reaction. *Spectrochim. Actaa* **2020**, *234*, 118249−118255.

(34) Sapkota, B.; Benabbas, A.; Lin, H. Y. G.; Liang, W. T.; Champion, P.; Wanunu, M. Peptide-Decorated Tunable Fluorescence Graphene Quantum Dots. *ACS Appl. Mater. Interfaces* **2017**, *9*, 9378−9387.

(35) Cai, G. N.; Yu, Z. Z.; Ren, R. R.; Tang, D. P. Exciton-Plasmon Interaction between AuNPs/Graphene Nanohybrids and CdS Quantum Dots/TiO₂ for Photoelectro- chemical Aptasensing of Prostate-Specific Antigen. *ACS Sensors* **2018**, *3*, 632−639.

(36) Cai, G. N.; Yu, Z. Z.; Tong, P.; Tang, D. P. Ti₃C₂ MXene quantum dot- encapsulated liposomes for photothermal immuno-assays using a portable near-infrared imaging camera on a smartphone. *Nanoscale* **2019**, *11*, 15659−15667.

(37) Ke, R.; Zhang, X. M.; Zhang, S. Y.; Li, S. L.; Mao, C. J.; Niu, H. L.; Song, J. M.; Tian, Y. P. Self-catalytic polymerization of a water-soluble selenium/polypyrrole nanocom- posite and its nonlinear optical properties. *Phys. Chem. Chem. Phys.* **2015**, *17*, 27548−27557.

(38) Strong, V.; Uribe, R. F. J.; Battson, M.; Kaner, R. Oriented Polythiophene Nanofi bers Grown from CdTe Quantum Dot Surfaces. *Small* **2012**, *8*, 1191−1196.

(39) Sharma, A.; Pandey, C. M.; Sumana, G.; Soni, U.; Sapra, S.; Srivastava, A. K. Chitosan encapsulated quantum dots platform for leukemia detection. *Biosens. Bioelectron.* **2012**, *38*, 107−113.

(40) Guo, Y. W.; Ge, X. S.; Guan, J.; Wu, L.; Zhao, F. H.; Li, H.; Mu, X. D.; Jiang, Y. J.; Chen, A. B. A novel method for fabricating hybrid biobased nanocomposites film with stable fluorescence containing CdTe quantum dots and montmorillonite-chitosan nanosheets. *Carbohyd. Poly.* **2016**, *145*, 13−19.

(41) Tan, L.; Wan, A.; Li, H.; Lu, Q. Novel quantum dots-carboxymethyl chitosan nanocomposite nitric oxide donors capable of detecting release of nitric oxide in situ. *Acta Biomater.* **2012**, *8*, 3744−3753.

(42) Vale, B. R. C.; Mourão, R. S.; Bettini, J.; Sousa, J. C. L.; Ferrari, J. L.; Reiss, P. Ligand induced switching of the band alignment in aqueous synthesized CdTe/ CdS core/shell nanocrystals. *Sci. Rep.* **2019**, *9*, 8332−8344.

(43) Wang, J. J.; Ke, K.; Zhang, X. M.; Zhang, S. Y.; Song, J. M.; Mao, C. J.; Niu, H. L.; Li, S. L.; Tian, Y. P. Self-catalytic synthesis of soluble polythiophene/tellurium nanocomposite and its nonlinear optical property. *Colloid poly. Sci.* **2016**, *294*, 1259−1267.

(44) Ryu, H. W.; Kim, Y. S.; Kim, J. H.; Cheong, I. W. Direct synthetic route for water dispersible polythiophene nanoparticles via surfactant-free oxidative polymerization. *Poly.* **2014**, *55*, 806−812.

(45) Pattavarakorn, D.; Jaesrichai, S.; Youngta, P.; Chaimongkol, P.; Thongbor, S. Electroactive Performances of Conductive Polythiophene/hydrogel Hybrid Artificial Muscle. *Energy Procedia* **2013**, *34*, 673−681.

(46) Shen, J. M.; Xu, L.; Lu, Y.; Cao, H. M.; Xu, Z. G.; Chen, T.; Zhang, H. X. Chitosan-based luminescent/magnetic hybrid nanogels for insulin delivery, cell imaging, and antidiabetic research of dietary supplements. *Int. J. Pharm.* **2012**, *427*, 400−409.

(47) Wang, Y.; Hou, Y. B.; Tang, A. W.; Feng, B.; Li, Y.; Teng, F. Synthesis and Optical Properties of Water Soluble CdTe Nanocrystals. *Acta Phys. Chim. Sin.* **2008**, *24*, 296−300.

(48) Grande, C. D.; Tria, M. C.; Jiang, G. Q. Surface-Grafted Polymers from Electro- polymerized Polythiophene RAFT Agent. *Macromolecules* **2011**, *44*, 966−975.

(49) Guzmán, D.; Isaacsb, M.; Tsukuda, T.; Yamazoe, S.; Takahata, R.; Schrebler, R.; Burgos, A.; Román, I. O.; Castillo, F. CdTe quantum dots modified electrodes ITO- (Polycation/QDs) for carbon dioxide reduction to methanol. *Appl. Surf. Sci.* **2020**, *509*, 145386−145395.

(50) Chen, X. J.; Wang, Y. Y.; Zhou, J. J.; Yan, W.; Li, X. H.; Zhu, J. J. Electrochemical Impedance Immunosensor Based on Three-Dimensionally Ordered Macroporous Gold Film. *Anal. Chem.* **2008**, *80*, 2133−2140.

(51) Li, J.; Zou, G. Z.; Hu, X. F.; Zhang, X. L. Electrochemistry of thiolcapped CdTe quantum dots and its sensing application. *J. Electroanaly. Chem.* **2009**, *625*, 88−91.

(52) Kang, J.; Li, X. W.; Geng, J. Y.; Han, L.; Tang, J. L.; Jin, Y.; Zhang, Y. H. Determination of hyperin in seed of Cuscuta chinensis Lam. by enhanced chemilumin- escence of CdTe quantum dots on calcein/K₃Fe[CN]₆ system. *Food Chem.* **2012**, *134*, 2383−2388.

(53) Jin, B. K.; Li, L.; Huang, J. L.; Zhang, S. Y.; Tian, Y. P.; Yang, J. X. IR Spectroelectrochemical Cyclic Voltabsorptometry and Deriva- tive Cyclic Voltabsorptometry. *Anal. Chem.* **2009**, *81*, 4476−4481.

(54) Shen, M.; Jia, W. P.; You, Y. J.; Hu, Y.; Li, F.; Tian, S. D.; Li, J.; Jin, Y. X.; Han, D. Luminescent properties of CdTe quantum dots synthesized using 3-mercaptopropionic acid reduction of tellurium dioxide directly. *Nanoscale Res. Lett.* **2013**, *8*, 253−258.

(55) Mansour, A. N.; Jonathan, K. K.; Waller, G. H.; Martin, C. A.; Zhang, C.; Qiao, X. Y.; Wang, Y. C.; Zhou, X. Y.; Balasubramanian, M. Structural Analysis of K₄Fe[CN]₆·3H₂O, K₃Fe[CN]₆ and Prussian Blue. *ECS J. Solid State SC* **2021**, *10*, 103002.

(56) Oku, M. Kinetics of photoreduction of Fe[III] in solid solution K₃(Fe, M)(CN)₆ (where M is Cr, Co) during XPS measurement. *J. Electron. Spectrosc.* **1994**, *67*, 401−407.

(57) Yamashita, T.; Hayes, P. Analysis of XPS spectra of Fe²⁺ and Fe³⁺ ions in oxide materials. *Appl. Surf. Sci.* **2008**, *254*, 2441−2449.

(58) Zeng, X. X.; Ma, S. S.; Bao, J. C.; Tu, W. W.; Dai, Z. H. Using Graphene-Based Plasmonic Nanocomposites to Quench Energy from Quantum Dots for Signal-On Photoelectrochemical Aptasensing. *Anal. Chem.* **2013**, *85*, 11720−11724.

(59) Chen, P. P.; Huang, K.; Dai, R.; Sawyer, E.; Sun, K.; Ying, B. W.; Wei, X. W.; Geng, J. Sensitive CVG-AFS/ICP-MS label-free nucleic acid and protein assays based on a selective cation exchange reaction and simple filtration separation. *Analyst* **2019**, *144*, 2797−2802.

(60) Jie, G. F.; Li, C. L.; Zhao, Y.; Kuang, Q.; Niu, S. Y. Fluorescent Mn:ZnCdS@ZnS and CdTe Quantum Dots Probes on SiO₂ Microspheres for Versatile Detection of Carcinoembryonic Antigen and Monitoring T4 Polynucleotide Kinase Activity. *ACS Appl. Nano Mater.* **2019**, *2*, 4637−4645.

(61) Qiu, Z. L.; Shu, J.; Tang, D. P. NaYF4:Yb, Er Upconversion Nanotrans- ducer with in Situ Fabrication of Ag₂S for Near-Infrared Light Responsive Photo- electrochemical Biosensor. *Anal. Chem.* **2018**, *90*, 12214−12220.

(62) Ma, X. M.; Wang, Z.; He, S.; Chen, C. Q.; Luo, F.; Guo, L. H.; Lin, Z. Y.; Qiu, B.; Chen, G. N.; Hong, G. L. Development of an Immunosensor Based on the Exothermic Reaction between H₂O and CaO Using a Common Thermometer as Readout. *ACS Sensors* **2019**, *4*, 2375−2380.

(63) Su, S.; Li, J.; Yao, Y.; Sun, Q.; Zhao, Q.; Wang, F.; Li, Q.; Liu, X. G.; Wang, L. H. Colorimetric Analysis of Carcinoembryonic Antigen Using Highly Catalytic Gold Nanoparticles-Decorated MoS₂ Nanocom- posites. *ACS Appl. Bio Mater.* **2019**, *2*, 292−298.